

# 1 Performance of a passive acoustic 2 linear array in a tidal channel

3 Matthew F. Auvinen, David R. Barclay

4 **Abstract**

5 Baseline ambient sound level assessment is important in quantifying anthropogenic noise contributions. Static  
6 acoustic sensing in high-flow conditions is complicated by pseudo-sound, or flow noise, caused by turbulent flow  
7 on the surface of a hydrophone. Signal processing methods are used to identify and suppress flow noise at low  
8 frequencies (< 500 Hz) in data collected on a four-element horizontal hydrophone array in Minas Passage, a tidal  
9 channel in the Bay of Fundy, in October 2016. Spectral slope analysis is used to identify the frequencies at which  
10 the flow noise and ambient noise contributions to the recorded signal are equal. The maximum frequencies at  
11 which flow noise is observed is determined using analysis of the spatial coherence. The array's performance in the  
12 Minas Passage is quantified by an empirical relationship between flow speed and the spectral critical frequencies  
13 of the coherent output from the linear array. Coherent averaging (broadside beamforming) is demonstrated as a  
14 potential flow noise suppression technique, improving low-frequency passive acoustic monitoring in a high-energy  
15 tidal channel.

16 **Index Terms**

17 Flow noise, ambient noise, array processing, tidal channel, and passive acoustic monitoring.

18 **I. INTRODUCTION**

19 **T**IDAL power utilities are currently leasing seafloor space within the Minas Passage in the Bay of  
20 Fundy with hopes of converting the energy of the region's tidal currents into electricity, a trend  
21 that has been supported by favorable projections of the Passage's tidal energy capacity [1]. It is important  
22 that these companies follow sustainable industry practices as the sector grows [2]. This includes the

Dr. David Barclay is an assistant professor in the Department of Oceanography, Dalhousie University. Matthew Auvinen holds a B.Sc. (Hons) from the Department of Oceanography, Dalhousie University, Halifax, NS (email: matthewauvinen@gmail.com; dbarclay@dal.ca).

Manuscript received June 26, 2017; revised MONTTH XX, 201X. This work was supported by the Natural Sciences and Engineering Research Council of Canada, GeoSpectrum Technologies, and Black Rock Tidal Power.

23 consideration of industry knowledge gaps, many of which are a consequence of the sector's immaturity [3].  
24 The uncertainty surrounding the ecological and environmental implications of tidal turbine infrastructure  
25 is a particularly important knowledge gap [4] and has qualified some opposition to turbine projects.

26 One of the main environmental concerns surrounding tidal turbine projects is the threat of physical  
27 contact and collision [5] [6]. The potential of this risk is largely due to uncertainty [7]. Indeed, the  
28 behavioural response of fish and marine mammals to the physical presence of tidal turbines is difficult  
29 to monitor and the relationship between tidal turbine infrastructure and local ecosystems is not fully  
30 understood. There is evidence that indicates seals actively avoid tidal turbines [8], suggesting that some  
31 marine mammals would not suffer from turbine strikes. However, this has not been tested with physical  
32 turbines. The uncertainty of other physical threats such as habitat alteration, interference with migrations,  
33 and disruption of sediment adds to the perceived risks associated with tidal turbines [4].

34 There are also acoustical concerns surrounding tidal energy. Turbines could become an important source  
35 of ambient noise in tidal channels through cavitation and mechanical noise [9]. Turbine anthropophony  
36 could affect animal navigation, communication, and predator-prey detections [10]. In some cases the sound  
37 generated by tidal turbines could even lead to physical harm [7]. While there is currently no evidence of  
38 turbine operational noise affecting marine animals, there may be risks associated with the noise emitted  
39 during the installation of tidal turbines, especially if pile driving is involved [4].

40 These environmental risks emphasize the need for baseline ambient noise measurements in the Minas  
41 Passage, against which turbine noise pollution can be measured. However, the utility of ambient sensing  
42 is limited by pseudo-sound, or flow noise, generated on the surface of a hydrophone in turbulent water.  
43 The masking effects of flow noise can complicate source identification and background noise assessment  
44 in high-flow settings, such as tidal channels.

45 Similar to turbulent flowing air [11], flowing water in a high Reynolds number regime generates pressure  
46 fluctuations on the surface of a hydrophone. These pressure fluctuations produce flow noise which is  
47 irregular, uncorrelated, and random. Local pressure fluctuations on the surface of a hydrophone represent  
48 near-field turbulence [12]. Free-drifting hydrophones moving with the mean water flow will experience  
49 little signal contamination, as it is the relative flow of water over a hydrophone's surface that leads to  
50 flow noise.

51 Flow noise follows a spectral slope of  $f^{-5/3}$  at low frequencies, behaviour that is analogous to Kol-  
52 mogorov's turbulence theory. This flow noise is not to be confused with wind-generated noise that produces

53  $f^{-5/3}$  spectral slopes at higher frequencies [13]. Bassett et al. [14] identifies  $f^{-5/3}$  flow noise below 20  
54 Hz and also describes steepened spectral slopes,  $f^{-m}$ , between 20 and 200 Hz. Lombardi [10] identifies  
55 the same steepened spectral slopes in measurements from the Grand Passage tidal channel. The flow  
56 noise that produces  $f^{-m}$  is a result of small-scale turbulence being averaged out across the surface of the  
57 hydrophones, which dampens (or reduces) measurements.

58 Flow noise presents a unique challenge for passive acoustic monitoring (PAM): a hydrophone in a  
59 high-flow setting will record both propagating sound and pseudo-sound. This suggests that models should  
60 distinguish between the two sound sources. While flow noise and ambient noise are inseparable, the  
61 masking effects of flow noise can be addressed by exploiting its uncorrelated nature. This has been done  
62 using ambient noise coherence, cross-correlation, and covariance [15] [16] [17].

63 Successful suppression of flow noise could benefit PAM systems in relatively energetic environments.  
64 The objectives of the present research are:

- 65 1) Use spectral analysis and spatial coherence to identify and characterize flow noise at low frequencies  
66 ( $< 500$  Hz).
- 67 2) Use coherent averaging (beamforming) to improve the performance of a linear hydrophone array  
68 by suppressing flow noise and enhancing the measurement of ambient noise.

69 This paper is organized as follows. Section II discusses important field work details, including an  
70 experiment description and instrumentation summary. Section III describes all relevant signal processing,  
71 with emphasis on spectral analysis, spatial coherence, and beamforming. Section IV presents the signal  
72 processing and data analysis results. Section V evaluates the results and identifies areas for future work.  
73 Lastly, Section VI summarizes the findings of the study in a series of conclusions.

## 74 II. FIELD WORK

75 Field work was completed on October 27, 2016, near the Fundy Ocean Research Center for Energy  
76 (FORCE) site in the Minas Passage of the Bay of Fundy. The FORCE site depth ranges between 40 and  
77 60 meters depending on the tide. The deployment period spanned roughly four hours, from 12:00 ADT  
78 to 16:00 ADT. This experimental window captured the transition from ebb tide to slack tide.

79 Wind speed was measured intermittently throughout the deployment period using a hand-held wind  
80 speed gauge. Throughout the observation period wind speed was low and the ocean surface was relatively  
81 calm. Tidal data was generated using a WebTide model [18].

82 There is a substantial fish population in the Minas Passage [5], some of which could contribute  
83 to the local ambient sound field [19]. Pilot whales, dolphins, seals, and other marine mammals that  
84 frequent the Minas Passage are another potential source of ambient noise. These animals generate sound  
85 through a variety of mechanisms, such as muscle action, stridulation, and vocalization [20]. Non-biological  
86 sound sources in the Minas Passage include wave action, anthropogenic activity, and bubbles. Proper  
87 characterization of the local sound field at the FORCE site would require consideration of these potential  
88 sound sources. However, their variability makes source identification challenging.

89 *A. Experiment*

90 A linear hydrophone array was streamed behind the *MV Nova Endeavour* (42' x 16'), which was  
91 anchored to the seafloor of the Minas Passage while in dead ship. The array was positioned roughly 15  
92 meters below the sea surface using a towfish depressor. The strength of the current kept the array at  
93 a relatively constant depth throughout the experiment. Four hydrophones were simultaneously sampled  
94 over a four hour period and processed by an analog-to-digital converter (ADC) on board the *MV Nova*  
95 *Endeavour*. The signal cable, which carried both the array and a drogue, was sheathed in a fairing to  
96 reduce strum generation and attached to a tow cable (6GA galvanized wire) using cable ties.

97 A drifting hydrophone (Geospectrum Technologies GuardBuoy) was deployed using a small auxiliary  
98 vessel launched from the *MV Nova Endeavour*. The GuardBuoy was suspended 2 meters below the surface  
99 using a drifting surface float and isolation system made of a damping mass, a Dacron non-stretch line,  
100 and a compliant bungee. The system isolated the recording hydrophone and instrument package from any  
101 surface action, such as the vertical movement of waves, which would otherwise generate mechanical or  
102 flow noise.

103 A total of five GuardBuoy casts were performed by driving the GuardBuoy upstream in a rigid-hulled  
104 inflatable boat (RHIB), turning off the RHIB engines, deploying the drifter, floating downstream in the  
105 RHIB alongside the drifter, and retrieving the drifter once it had reached 20 meters beyond the array. A  
106 separation distance of at least 10 meters was maintained between the drifter and the RHIB while floating  
107 downstream. It is important to note that the drifter transects passed over the array.

108 These transects were performed over the course of three hours, beginning at 13:00 ADT. The GuardBuoy  
109 signals are assumed to be free of flow noise and were used as benchmarks to assess the performance  
110 of the array. The turbulent tidal channel is assumed to be well mixed with an isovelocity sound speed  
111 profile, minimizing noise field variability over the depth difference between the two systems.

112 *B. Instrumentation*

113 The linear array is an oil-filled array with a rigid exterior and acoustically transparent outer skin.  
 114 It contains four sequentially spaced hydrophones with a horizontal configuration along the axis of the  
 115 array. The array and the hydrophones were constructed by GeoSpectrum Technologies. Each neighbouring  
 116 hydrophone is separated by a distance  $d = 17\text{cm}$ . The array hydrophones were set to simultaneously sample  
 117 at a rate of 96 kHz with an acoustic bandwidth of 48.019 kHz. The four channels on the array continuously  
 118 recorded 10 minute WAV files over a 4 hour period. Power spectra were calibrated to dB re  $1 \mu\text{Pa}^2/\text{Hz}$   
 119 according to frequency-dependent sensitivities supplied by the manufacturer. The GuardBuoy sampled at  
 120 a rate of 96 kHz with an acoustic bandwidth of 48 kHz, and was equipped with a GPS to record transect  
 121 geospatial information. The Guard Buoy recorded WAV files in 30 minute segments. Corresponding power  
 122 spectra were converted to dB re  $1 \mu\text{Pa}^2/\text{Hz}$  according to frequency-dependent sensitivities supplied by the  
 123 manufacturer.

124 **III. DATA ANALYSIS**

125 Data analysis was performed in MATLAB in several stages. The analysis began with the calculation of  
 126 the power spectral density (PSD) from the raw WAV files, followed by spectral analysis, spatial coherence  
 127 analysis, and broadside beamforming.

128 *A. General Signal Processing*

The output of a hydrophone is defined as

$$x_i(t) = \sigma_i(t) + n_i(t) \quad (1)$$

129 where  $x_i$  is the recorded time series on each  $i$ th hydrophone,  $\sigma_i$  is the sound field's ambient components,  
 130 and  $n_i$  is the locally generated flow noise. Importantly,  $n_i$  and  $\sigma_i$  are uncorrelated. Furthermore, the  
 131 inherent randomness of flow noise makes  $n_i$  incoherent with respect to  $n_j$ .

132 The power spectrum, or spectral density, is defined as

$$S_{ii}(\omega) = \frac{\langle X_i(\omega) \cdot X_i^*(\omega) \rangle}{T} \quad (2)$$

133 where  $X_i$  is the Fourier transform of  $x_i$ ,  $\omega$  is angular frequency,  $*$  denotes a complex conjugate,  $\langle \rangle$   
 134 indicates an ensemble average, and  $T$  is the observation interval. All Fourier transforms are windowed by

135 a Hann function and the Hann function's effect on the variance has been accounted for. The time series  
 136 were divided into 34.1 second-long segments, where each segment was further split into 50 contiguous  
 137 subsegments of 0.682s with no overlap. A  $2^{16}$  Fourier transform was applied to each subsegment, from  
 138 which ensemble averaging produced a power spectral density with a frequency bin width of 1.47 Hz.  
 139 Coherence is used to quantify the similarity between two signals and is defined as

$$\Gamma_{ij}(\omega) = \frac{S_{ij}(\omega)}{(S_{ii}(\omega) \cdot S_{jj}(\omega))^{\frac{1}{2}}}. \quad (3)$$

140 *B. Power Spectrum Probability Density*

141 Spectral probability density (SPD) is an analytical technique used to depict the variability of the power  
 142 spectrum over a period that is much longer than the minimum time required for a stationary measurement  
 143 of power to be made [21]. This form of analysis facilitates the identification of unique events within a  
 144 series of spectra. The power spectrum probability density (PSPD) is defined as

$$\text{PSPD}(f) = H(S_{ii}(f), h) \quad (4)$$

145 where  $\text{PSPD}(f)$  is the power spectrum probability density at frequency  $f$ , and  $H(S(f), h)$  is the histogram  
 146 of the power spectrum  $S_{ii}$  at frequency  $f$  with a histogram bin width of  $h$  dB re  $1 \mu\text{Pa}^2/\text{Hz}$ . By combining  
 147 PSPD results across frequencies, we generate a PSPD matrix

$$\begin{bmatrix} \text{PSPD}(f_1) & \text{PSPD}(f_2) & \text{PSPD}(f_3) & \dots & \text{PSPD}(f_a) \end{bmatrix} \quad (5)$$

148 where  $\text{PSPD}(f_a)$  is the PSPD at the  $a$ th frequency.

149 *C. Spectral Critical Frequency*

150 Lombardi [10] and Bassett et al. [14] suggest that there are three distinct spectral slope regions in  
 151 the low-to-mid-frequency range: spectral slopes of Kolmogorov's  $f^{-5/3}$ ; steepened flow noise spectral  
 152 slopes,  $f^{-m}$ , that include the effects of a finite volumed sensor [14]; and an ambient noise region that is  
 153 determined by near-field and far-field ambient sound sources.

154 The local spectral slope is defined as

$$-M = \frac{S_{ii}(2\pi f_a) - S_{ii}(2\pi f_b)}{\log(f_a \cdot f_b^{-1})} \quad (6)$$

where  $S_{ii}(2\pi f_a)$  is the spectral density on the  $i$ th sensor at frequency  $f_a$  and  $S_{ii}(2\pi f_b)$  is the spectral density on the  $i$ th sensor at frequency  $f_b$ . The spectral slope in dB/decade is described by (6).

The transition from the flow noise region of  $f^{-m}$  to the ambient noise region is marked by the frequency knee, where the spectral slope begins to shallow. That is, the exit from the flow noise region is marked by a deviation below the slope  $f^{-m}$ . Here, the spectral critical frequency,  $f_c$ , is defined as the first frequency at which

$$|M| < |m| \quad (7)$$

is true. Both slopes in (7) are in dB/decade.

#### 162 D. Coherence Critical Frequency

163 Spatial coherence is calculated for each channel combination using (3), providing an assessment of  
 164 signal similarity between elements. Propagating ambient noise is highly correlated across the array.  
 165 Additionally, propagating noise at wavelengths sufficiently large relative to element spacing produces  
 166 very high coherence at low frequencies by effectively co-locating sensors. Conversely, flow noise is a  
 167 source of incoherence, as pseudo-sound is uncorrelated across the linear array (when turbulent scales are  
 168 smaller than hydrophone separation). Therefore, in the band  $f < 500$  Hz, flow noise is marked by low  
 169 coherence while ambient noise is marked by high coherence. The transit of this coherence boundary, from  
 170 flow noise (incoherent) to ambient noise (coherent) provides a metric for describing the extent of flow  
 171 noise across the array.

172 The coherence critical frequency,  $f'_c$ , is defined as the frequency at which a minimum coherence  
 173 threshold is crossed due to flow noise masking. To establish this coherence threshold, we assume an  
 174 isotropic ambient noise field such that the horizontal coherence is given by Buckingham [22]

$$G_{ij}(\omega') = \frac{\sin(\omega'_{ij})}{\omega'_{ij}} \quad (8)$$

175 where

$$\omega'_{ij} = \frac{2\pi d_{ij} f}{c}. \quad (9)$$

176 Here,  $d_{ij}$  is the separation distance between the  $i$ th and  $j$ th hydrophone and  $c$  is the local sound speed.

177 We define  $f'_c$  as the first frequency at which

$$|\Gamma_{ij}(\omega')| \geq 0.9 \cdot G_{ij}(\omega') \quad (10)$$

178 is true. We can be confident that any coherence within 10% of (8) is real and significant while any drop  
 179 below the threshold given by the right hand side of (10) is caused by the addition of flow-generated  
 180 incoherent noise. This automated critical frequency detector corresponds to a coherence threshold of  $\sim$   
 181 0.9. The use of a more sophisticated noise model such as Cron and Sherman [23] or Deane et al. [24] in  
 182 the place of (8) yields a nearly identical threshold.

183 *E. Linear Regression*

184 Least squared linear regressions between critical frequencies,  $f_c$  and  $f'_c$ , and flow speed,  $u$ , are used to  
 185 identify and characterize the prevalence of flow noise and ambient noise in measurements.

186 *F. Beamforming*

187 We use a broadside beamformer to coherently average the channels across the array. Locally generated  
 188 flow noise and the ambient sound field are inseparable, however we can describe their relative prevalence  
 189 with the theoretical signal-noise ratio (SNR) where we are defining ambient sound as the signal, and flow  
 190 noise as the noise. By taking the Fourier transform of (1) and substituting into (2), we find

$$S_{ii} = \frac{\langle (\zeta_i + N_i) \cdot (\zeta_i^* + N_i^*) \rangle}{T} \quad (11)$$

191 where  $\zeta_i$  and  $N_i$  are the Fourier transforms of  $\sigma_i$  and  $n_i$ , respectively. For clarity, the frequency dependency  
 192 has been omitted. Since  $\zeta_i$  and  $N_i$  are uncorrelated, we can expand (11) to arrive at

$$S_{ii} = \frac{\langle \varsigma_i \varsigma_i^* \rangle + \langle N_i N_i^* \rangle}{T}. \quad (12)$$

193 Given (12), the SNR for a single hydrophone ( $\text{SNR}_H$ ) is defined as

$$\text{SNR}_H = \frac{\langle \varsigma_i \varsigma_i^* \rangle}{\langle N_i N_i^* \rangle} \quad (13)$$

194 where  $\text{SNR}_H = 1$  at the critical frequency,  $f_c$ . Now consider an array of hydrophones indexed by  $i$ , where  
195 the ambient sound field component of the signal on each phone is

$$\sigma_{i+1}(t) = \sigma_1(t - \tau_i) \quad (i > 1) \quad (14)$$

196 where

$$\tau_i = \frac{i \cdot d \cos \theta}{c} \quad (15)$$

197 is the acoustic travel time in seconds for plane wave noise arriving on the sensors at the angle  $\theta$ . Here,  
198  $d$  is the nearest neighbour element separation. Taking the Fourier transform of (14) gives

$$\varsigma_i(\omega) = \varsigma_1(\omega) e^{-i\omega\tau_i}. \quad (16)$$

199 The coherent sum of the signals across the array is defined as

$$x_T(t) = \sum_{i=1}^l x_i(t) \quad (17)$$

200 where  $x_i(t)$  is the signal recorded on the  $i$ th element of a linear array  $l$  elements long. Since no time  
201 delay has been applied to  $x_i(t)$ ,  $x_T(t)$  is the equivalent to beamforming broadside to the array. Since the  
202 source of interest is ambient noise, the sound field is assumed to be axially symmetric. Thus the horizontal  
203 array orientation and beam direction are unimportant, provided an appropriate array gain compensation

204 is applied.

205 The Fourier transform of (17) is

$$X_T(\omega) = \sum_{i=1}^l X_i(\omega). \quad (18)$$

206 The array power spectral density can be estimated using (18) by

$$A = \frac{\langle X_T(\omega) \cdot X_T^*(\omega) \rangle}{T}. \quad (19)$$

207 Given an array with both ambient noise and flow noise components, (18) can be expanded to

$$X_T = [\varsigma_1 + N_1 + \varsigma_2 + N_2 + \dots + \varsigma_l + N_l] \quad (20)$$

208 which describes the total output of all sensors on an array with  $l$  elements. Substituting (16) into (20)  
209 gives

$$X_T = \varsigma_1 + N_1 + \sum_{i=1}^l (\varsigma_1 e^{-i\omega\tau_i} + N_{i+1}). \quad (21)$$

210 Using the Fourier transform of the coherently summed outputs across the array, the power spectral density  
211 can be computed by substituting (21) into (19) yielding

$$A = \frac{\langle \varsigma_1 \varsigma_1^* \left[ l + \sum_{i=1}^{l-1} \frac{1}{2} (l-i) \cos(\omega\tau_i) \right] + N \cdot N^* \rangle}{T} \quad (22)$$

212 where

$$N = \sum_i^l N_i \quad (23)$$

213 is the coherently summed flow noise. This term can be simplified by assuming the power of the flow  
214 noise measured on each individual hydrophone is equal across the array,

$$\langle N_i N_i^* \rangle = \langle N_j N_j^* \rangle \quad (24)$$

<sup>215</sup> and uncorrelated between the sensors,

$$\langle N_i N_j^* \rangle = \delta_{ij} \cdot N_1 N_1^* \quad (25)$$

<sup>216</sup>

$$\delta_{ij} = \begin{cases} 0 & \text{if } i \neq j \\ 1 & \text{if } i = j. \end{cases}$$

<sup>217</sup> Then the total power received by the array becomes

$$A = \frac{\langle \zeta_1 \zeta_1^* \rangle \left[ l + \sum_{i=1}^{l-1} \frac{1}{2} (l-i) \cos(\omega \tau_i) \right] + l \langle N_1 N_1^* \rangle}{T}. \quad (26)$$

<sup>218</sup> Furthermore, if  $K$  is defined as

$$K = l + \sum_{i=1}^{l-1} \frac{1}{2} (l-i) \cos(\omega \tau_i) \quad (27)$$

<sup>219</sup> then (26) becomes

$$A = \frac{K \langle \zeta_1 \zeta_1^* \rangle + l \langle N_1 N_1^* \rangle}{T} \quad (28)$$

<sup>220</sup> where (28) describes the array spectral density. Here,  $SNR_A$  describes the relative strength of the ambient  
<sup>221</sup> noise and flow noise components of the array output, such that

$$SNR_A = \frac{K \langle \zeta_1 \zeta_1^* \rangle}{l \langle N_1 N_1^* \rangle}. \quad (29)$$

<sup>222</sup> Comparing (29) to the result derived for a single hydrophone, given by (13), we see that the beamformed  
<sup>223</sup> array improves the signal-to-noise ratio by a factor of  $\frac{K}{l}$ . Furthermore, (29) suggests that array performance

improves with an increasing number of hydrophones,  $l$ . For an array with 4 elements, at broadside,  $\frac{K}{l} = \frac{7}{4}$ .

### 226 G. Array Gain

227 The broadside beamforming analysis applied to the linear array generates artificial spectral density gain.  
 228 As a result, an array gain formula is applied to the beamformed results to correct the inflated values. The  
 229 array gain formula presented here is adapted from Cox [25], such that

$$AG = 10 \log l. \quad (30)$$

230 The array gain correction is performed by subtracting the result of (30) from the calculated array power  
 231 spectral density.

### 232 H. Algorithm Assessment

233 All channel signals are consolidated into one coherent array output using (18) and (19). The resulting  
 234 coherent array signal is compared to signals from the GuardBuoy and a single fixed hydrophone to evaluate  
 235 the performance of the beamformed array. The algorithm is further tested by comparing the coherent array  
 236 spectral critical frequencies to the spectral critical frequencies of a fixed single hydrophone.

## 237 IV. RESULTS

### 238 A. Spectral Density

239 A comparison between spectral density and current speed (Fig. 1) reveals high signal levels in fast  
 240 flowing water and low signal levels in slow flowing water. The signal power is high below 10 Hz and falls  
 241 off as the frequency approaches 100 Hz, which indicates that flow noise is prevalent at low frequencies.

242 The hydrophone power spectrum contains multiple episodes of mid-frequency noise. These signals are  
 243 attributed to ship noise generated by passing ships and the small vessel used in the GuardBuoy drifter  
 244 tests. The abrupt shift in spectral density at 90 minutes is attributed to a reset of the ground between the  
 245 data acquisition hardware and the array housing. The data collected during this reset have been omitted.

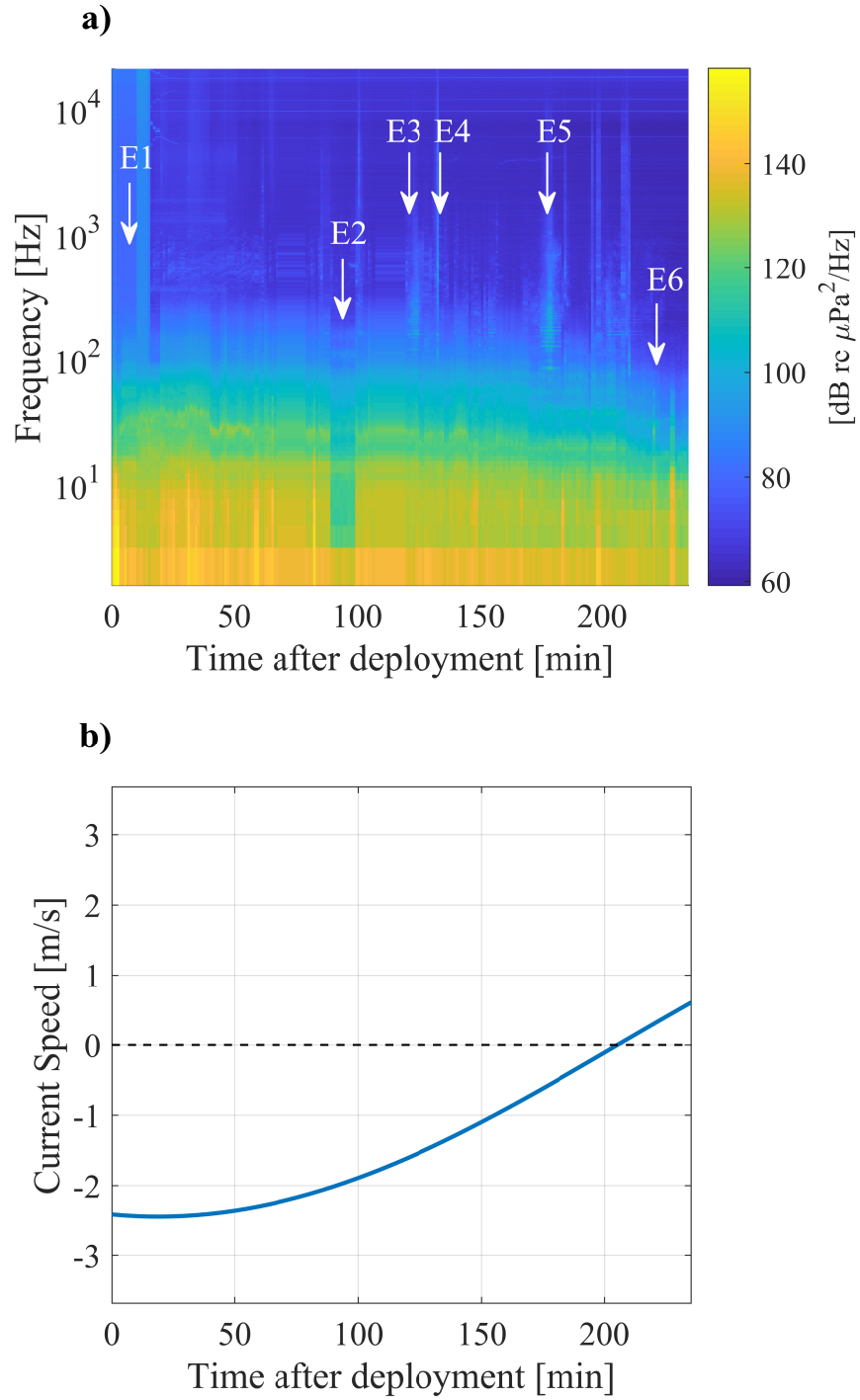


Fig. 1. Power spectrum for channel 0 on the array (a). The spectrum is plotted over the deployment period across a range of low-to-mid frequencies. Data sampling errors are marked by E1 and E2 and different mid-frequency noise events, such as ship noise, are marked by E3 - E6. The data from these events has been omitted from the spectral and coherence analyses. The spectrum begins at maximum ebb tide and ends shortly after slack tide, as shown by the current speed time series (b). Power decreases with current speed over the deployment period.

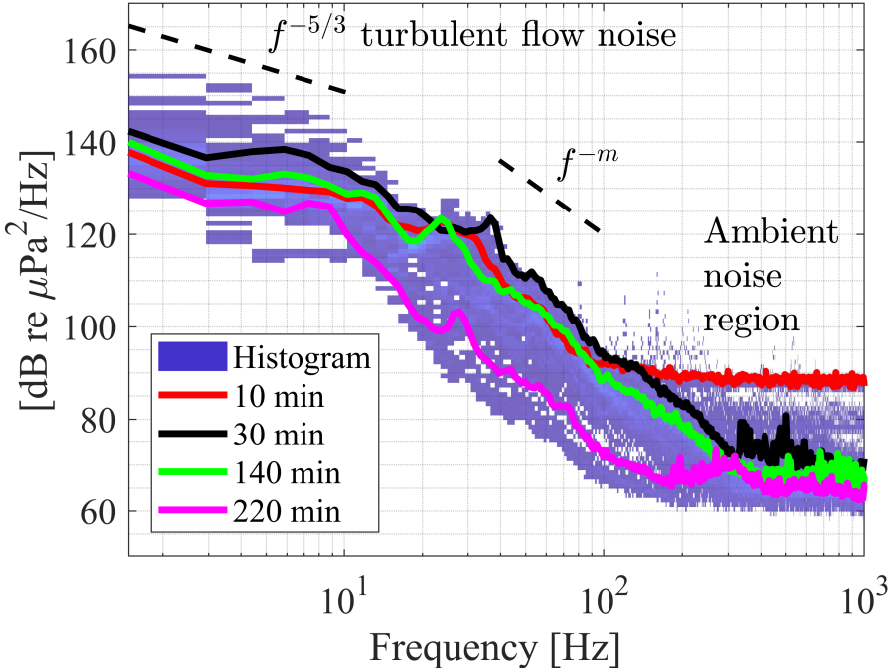


Fig. 2. Fixed single hydrophone power spectrum probability density over the entire deployment period. Turbulent flow noise is prevalent  $< 10 \text{ Hz}$  (where wavelengths  $\gg$  sensor size), with a spectral slope of  $f^{-5/3}$ , while turbulence interacting with the hydrophone's finite volume (in the  $10 \text{ Hz}$  to  $100 \text{ Hz}$  band) yields a spectral slope of  $f^{-m}$ . The ambient sound field dominates at frequencies  $> 300 \text{ Hz}$ . Coloured lines represent individual spectra recorded at the time after deployment indicated in the legend.

#### 246 B. Power Spectrum Probability Density

247 The PSPD (Fig. 2) facilitates the broad-scale assessment of a hydrophone's spectral density over entire  
 248 deployment periods. The PSPD follows a spectral slope of  $f^{-5/3}$  below  $10 \text{ Hz}$ , behaviour analogous to  
 249 Kolmogorov's turbulence theory. This spectral slope marks a region of flow noise within the signal. A  
 250 steepened spectral slope of  $f^{-m}$ , where  $m > \frac{5}{3}$ , persists between  $40$  and  $100 \text{ Hz}$ , a result of small-scale  
 251 turbulence when turbulence wavelength  $\ll$  sensor size. This small-scale turbulence is averaged out over  
 252 the surface of the hydrophone sensor, dampening the measured signals. The PSPD results show that  
 253 ambient noise is dominant above  $300 \text{ Hz}$ , where signal levels are markedly low. Single power spectra are  
 254 superimposed on the PSPD and suggest that measurements in slow current conditions contain a greater  
 255 extent of ambient noise relative to those in fast current conditions.

256 Early in the deployment (around  $10$  minutes) electronic noise in the system raised the noise floor to  $90$   
 257  $\text{dB } \mu\text{Pa}$ . While this was quickly remedied on site and has been accounted for in the data, a noise floor  
 258 persisted around  $60 \text{ dB } \mu\text{Pa}$ .

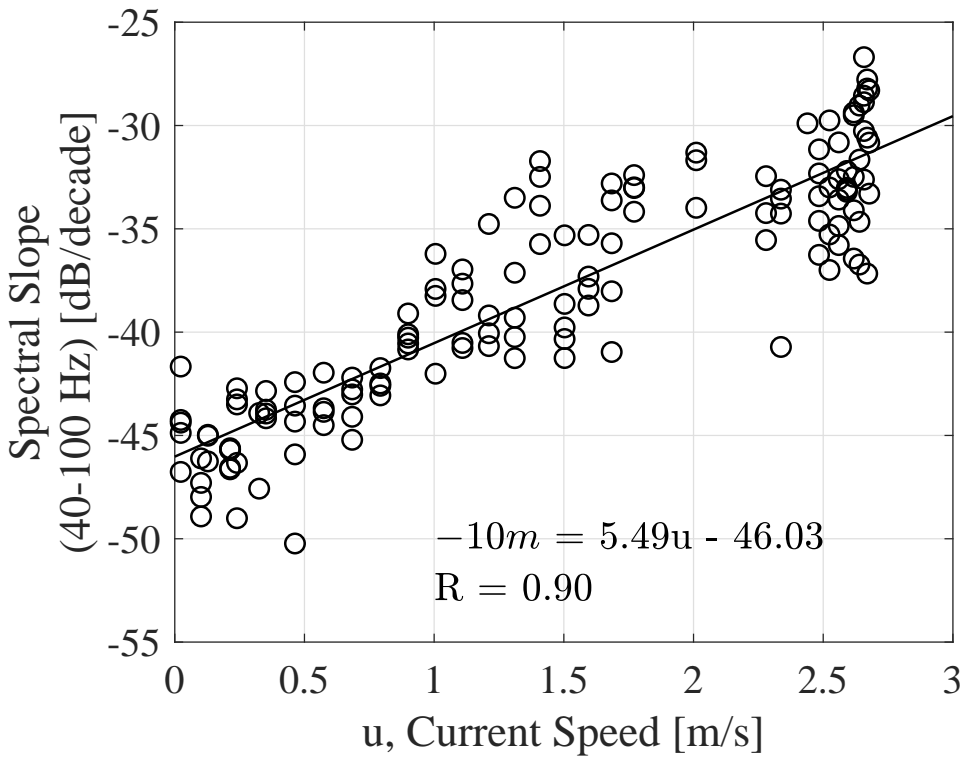


Fig. 3. Relationship between spectral slope,  $m$ , and current speed,  $u$ , between 40 and 100 Hz for channel 0. Spectral slope magnitude increases with decreasing flow. The correlation coefficient,  $R$ , is reported.

### 259 C. Spectral Critical Frequency

260 Spectral slopes were calculated between 40 and 100 Hz for each minute of deployment using (6). The  
 261 linear relationship between spectral slope,  $m$ , and current speed,  $u$ , (Fig. 3) indicates that signals recorded  
 262 in decreasing flow are increasingly damped (steepened slope). The inverse relationship between current  
 263 speed and spectral slope suggests that signals are less damped in fast flowing water, a result of larger  
 264 turbulence scales. The spectral slopes observed between 40 and 100 Hz range from -25 to -60 dB/decade.  
 265 The correlation coefficient,  $R$ , indicates that there is a meaningful correlation between spectral slope and  
 266 current.

267 The spectral critical frequency is the frequency at which flow noise and ambient noise are equal in  
 268 power, and was calculated for each minute of deployment using (7). These critical frequencies were  
 269 regressed against current speed, as shown in Fig. 4. There is a positive correlation between spectral  
 270 critical frequency and current speed, where fast flow coincides with high spectral critical frequencies.

271 The intercepts have not been forced to zero. This is because it is unrealistic to expect that we can com-  
 272 pletely eliminate flow noise, or low-frequency noise generated by the mechanical systems that comprise  
 273 the tow body. If this were a moored system with no surface expression, that assumption might be valid,

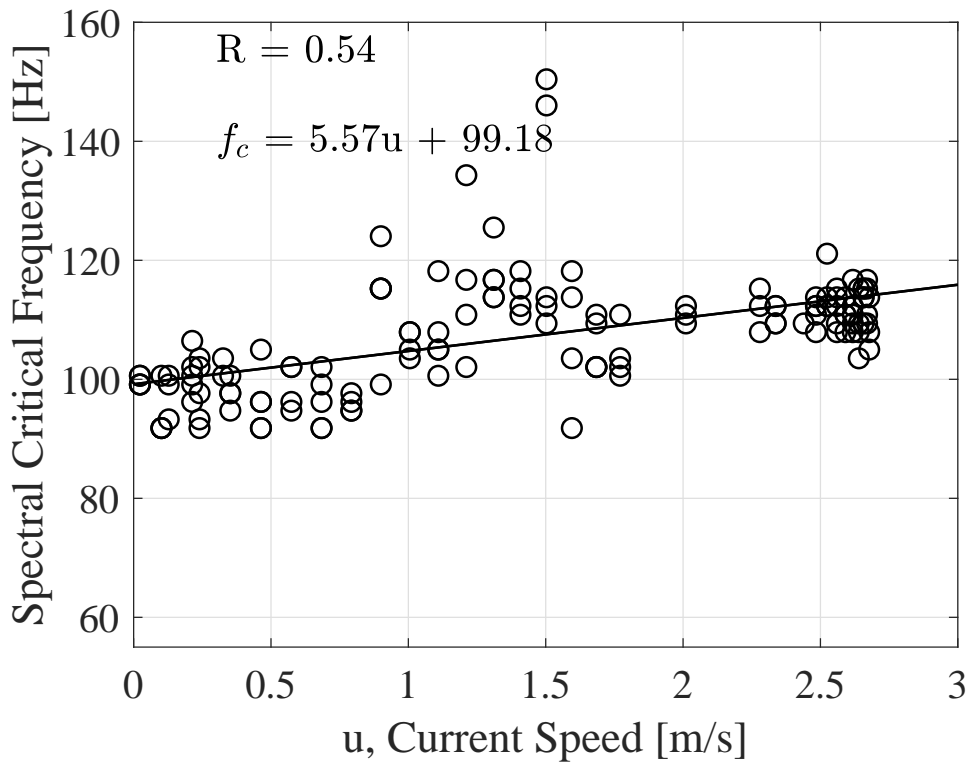


Fig. 4. Relationship between spectral critical frequency,  $f_c$ , and current speed,  $u$ , for channel 0. Spectral critical frequency marks where the flow noise and ambient noise contributions to the recorded signal are equal, and increases with current speed. The correlation coefficient,  $R$ , is reported.

274 but is not considered here.

#### 275 D. Spatial Coherence

276 Spatial coherence is calculated for different hydrophone combinations across the linear array using  
 277 (3). The spatial coherence results are presented in magnitude coherence for the entire deployment period  
 278 (Fig. 5). If the wavelength of propagating sound is sufficiently long (frequency sufficiently low) the  
 279 sensors would become relatively co-located and the coherence would tend to unity. However, the results  
 280 suggest that the low frequency data is overwhelmingly incoherent, since the locally generated flow noise  
 281 is incoherent from one hydrophone to the next.

282 Flow noise is uncorrelated and propagating ambient noise is highly correlated at low frequencies. As  
 283 a result, low coherence and high coherence are a sign of flow noise and ambient noise, respectively.  
 284 Therefore, the spatial coherence results are partitioned into two distinct regions: a flow noise region  
 285 and an ambient noise region. Visual assessment suggests that flow noise is consistently present at low  
 286 frequencies and can be prominent at higher frequencies (above 600 Hz). The ambient noise region is  
 287 present between 200 and 600 Hz and contains the same vessel noise identified in Fig. 2.

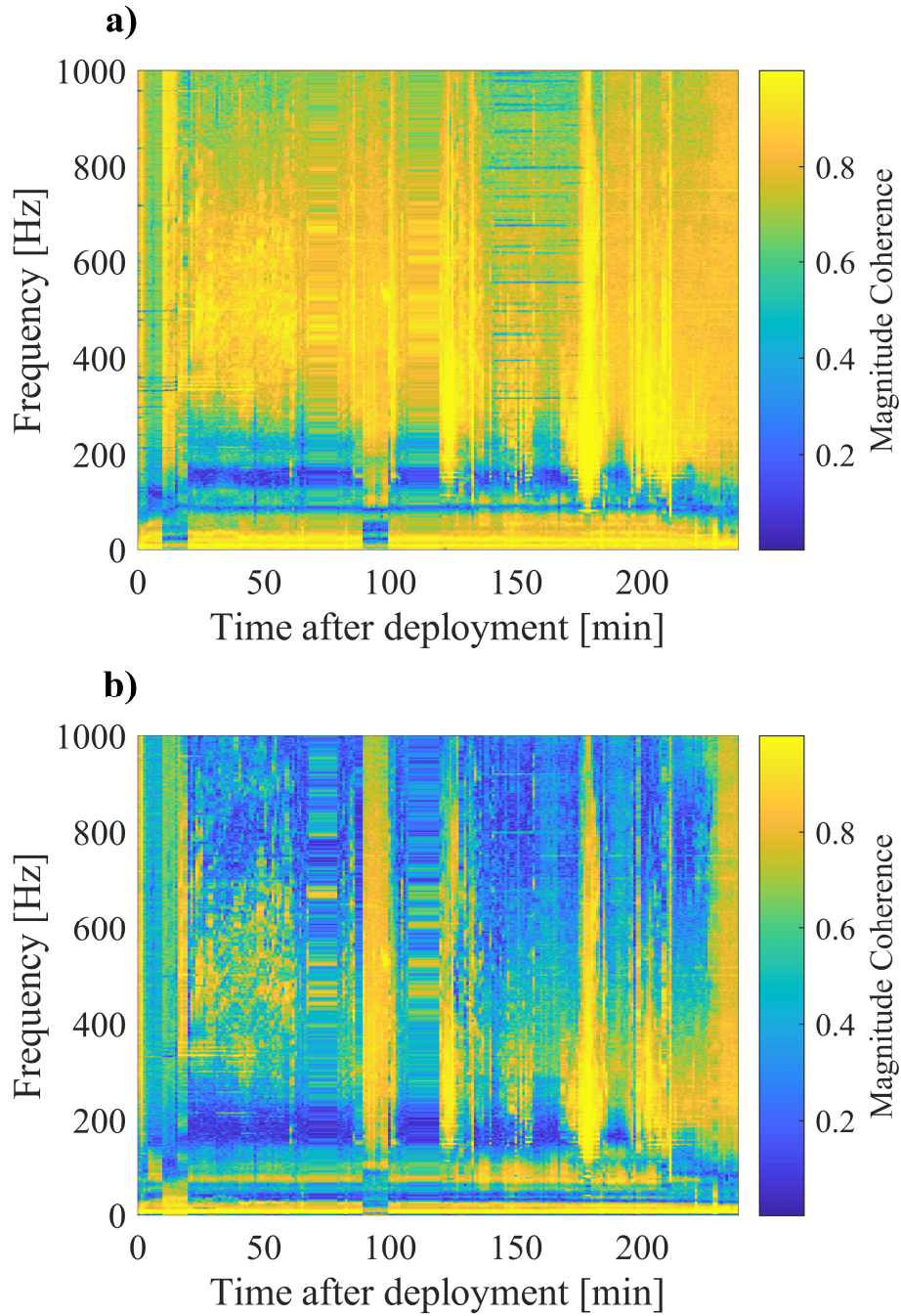


Fig. 5. Spatial coherence over the experimental period. Magnitude coherence is expected to tend to unity as the fixed hydrophones become relatively co-located. However, uncorrelated flow noise on each phone breaks that relationship. The extent of incoherent flow noise increases with current speed. Channel 0 - 1 (a) and 0 - 3 (b) are shown as examples. Results hold to all other channel combinations.

288 *E. Coherence Critical Frequency*

289 The coherence critical frequency is the highest frequency at which flow noise can be detected. The  
290 coherence critical frequency was calculated for each minute of deployment for each combination of chan-

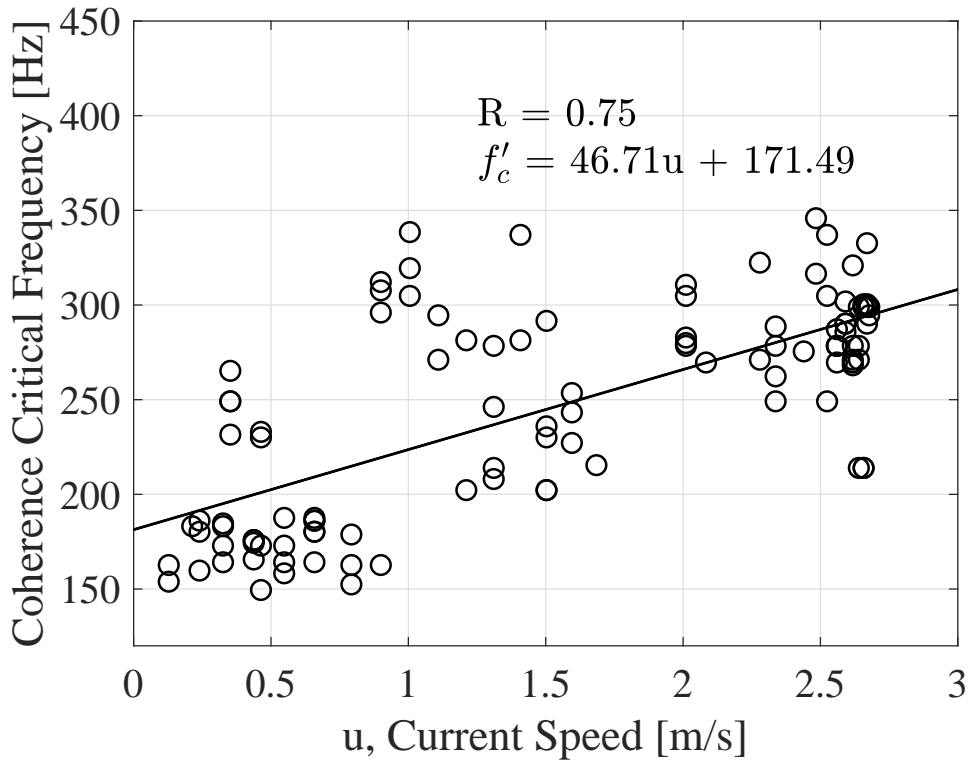


Fig. 6. Relationship between coherence critical frequency,  $f'_c$ , and current speed,  $u$ , for channels 0 - 1. Coherence critical frequency is the highest frequency at which flow noise can be detected, and increases with current speed.

nels, and is used to quantify the relative prevalence of flow noise and ambient noise within a measurement (Fig. 6). The coherence critical frequency is a more sensitive method of flow noise measurement than the spectral critical frequency, as spatial coherence is used as an indicator of flow noise cessation rather than relative noise contributions. The coherence critical frequency increases with increasing flow speed, a relationship similar to that of the spectral critical frequency.

It is important to note that the coherence is impacted by any temporary deterministic noises present in the sound field, such as the auxiliary RHIB, mechanical array noise, or noise generated aboard the *MV Nova Endeavour*. In such instances, the automated coherence critical frequency detector fails, and yields an outlier. These outliers have been removed.

#### 300 F. Beamforming

The spectral critical frequency of the coherent array output is compared to the fixed single hydrophone spectral and coherence critical frequencies in Fig. 7. The standard deviations of the spectral slope and spatial coherence critical frequency regressions were extracted from the averaged fits, while the standard

304 deviation of the coherent array critical frequency regression was calculated from the data during the  
305 regression.

306 The coherence critical frequencies are relatively high, while spectral critical frequencies (both fixed  
307 single hydrophone and coherent array) are relatively low. This is attributed to the more sensitive nature  
308 of the coherence-based method. Above coherence critical frequencies we can be confident that there  
309 is no contamination of the ambient noise field by flow noise. Conversely, the fixed single hydrophone  
310 and coherent array spectral critical frequencies show where flow noise and ambient noise have equal  
311 power. The coherence and spectral critical frequencies serve as the respective upper and lower bounds of  
312 different noise regimes. The coherent array output contains lower critical frequencies than the fixed single  
313 hydrophone, indicating that the broadside beamforming approach lessens the extent of flow noise within  
314 the measurements.

315 Fig. 8 compares GuardBuoy, fixed single hydrophone, and horizontal coherent array power spectra at 1.5  
316 hours into the experiment. At this time the drifter and array were in close proximity and the current was  
317 2.2 m/s. The GuardBuoy spectrum behaves differently from the rest, exhibiting lower levels at frequencies  
318 below 100 Hz. A pronounced excursion in spectral slope is present at 10 Hz in the GuardBuoy spectrum,  
319 suggesting non-negligible flow noise is affecting the drifter's low-frequency measurements. This is typical  
320 of all moored or free drifting passive acoustic systems that have a surface expression or subsurface float.  
321 The fixed single hydrophone shows clear symptoms of flow noise at low frequencies.

322 The spectra reveal that the coherent array spectra transitions to the ambient noise region at lower  
323 frequencies than the fixed single hydrophone. Furthermore, the coherent array signal levels are relatively  
324 lower than the fixed single hydrophone levels at all low frequencies, indicating moderate flow noise  
325 suppression. There is reasonable agreement between the GuardBuoy and coherent array above the critical  
326 frequency, with some difference above 700 Hz. This disparity is attributed to the lack of co-location  
327 between the array and the GuardBuoy, as they are vertically and horizontally displaced relative to each  
328 other.

## 329 V. DISCUSSION

### 330 A. Spectral Critical Frequency

331 Results show that critical frequency and flow speed are positively related, giving the intuitive result  
332 that flow noise is prevalent in fast current conditions. The spectral critical frequency presents a method  
333 of identifying flow noise prevalence within a signal.

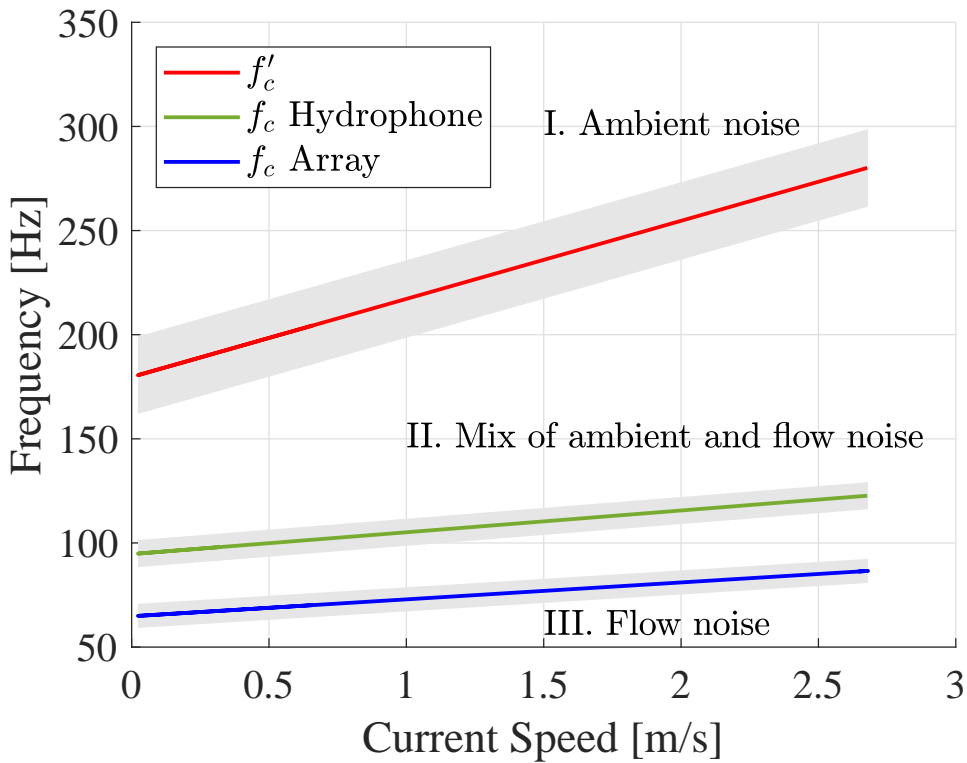


Fig. 7. Comparison of fixed single hydrophone spectral critical frequency (green), array spectral critical frequency (blue), and coherence critical frequency (red) as a function of current speed. Uncertainties are one standard deviation (shaded). Coherence critical frequency,  $f'_c$ , separates region I, where flow noise is negligible, and region II, where flow and ambient noise are both present, while spectral critical frequency,  $f_c$ , separates regions II and III, where flow noise dominates. The coherent array effectively suppresses flow noise, as indicated by its lower boundary relative to the fixed single hydrophone.

334 The spectral critical frequency marks where ambient noise and flow noise have equal power, and  
 335 provides two important insights. Firstly, frequencies above the spectral critical frequency will contain a  
 336 mixture of ambient noise and flow noise. Secondly, frequencies below the spectral critical frequency will  
 337 be dominated by flow noise, since measurements in these frequencies contain spectral slopes that align  
 338 with turbulence theory. These insights are important, as they provide useful context for future signal level  
 339 and sound-source evaluations in tidal channel measurements.

340 *B. Spatial Coherence*

341 Spatial coherence results for different sensor combinations show that there are two distinct coherence  
 342 regions across the array: an incoherent flow noise region and a coherent ambient noise region. The  
 343 prevalence of these regions is quantified with the coherence critical frequency. Moreover, the coherence  
 344 critical frequency marks the frequency above which flow noise is absent. A least squared regression reveals  
 345 that there is a positive relationship between flow speed and coherence critical frequency.

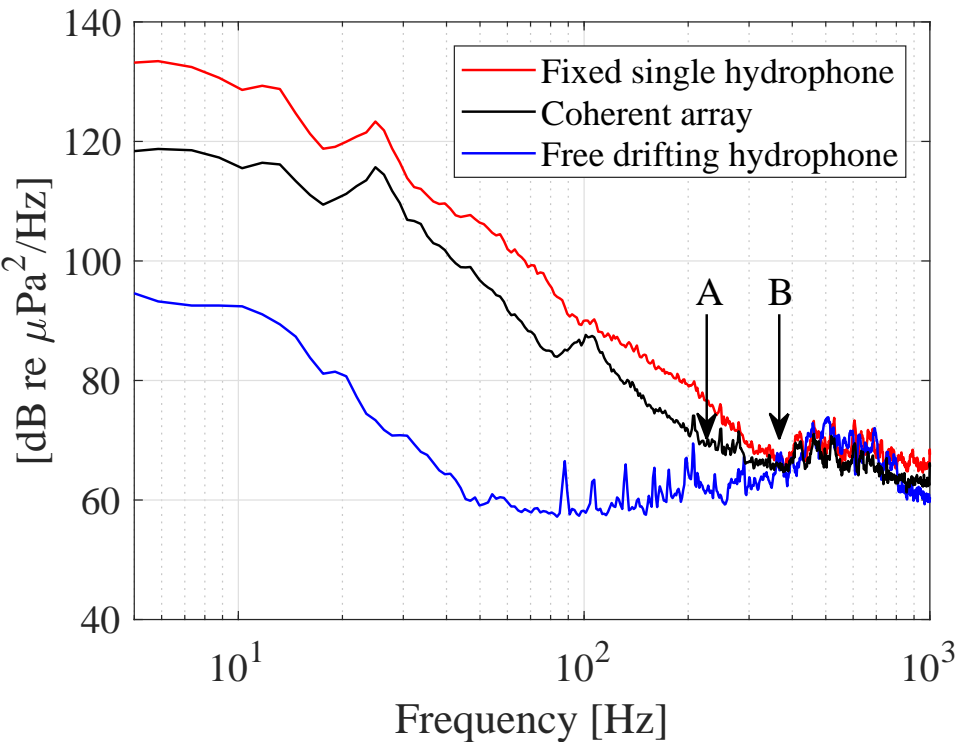


Fig. 8. Comparison of fixed single hydrophone (red), coherent array (black), and free drifting hydrophone (blue) signal power spectra at 1.5 hr into the deployment. The current speed at this moment was 2.2 m/s. A and B indicate the spectral critical frequencies of the coherent array and the fixed single hydrophone, respectively. The reduced levels and spectral critical frequency of the coherent array output relative to the fixed single hydrophone indicates flow noise suppression.

346 The spectral critical frequency provides a lower boundary, below which ambient noise is negligible,  
 347 and the coherence critical frequency provides an upper boundary, above which flow noise is negligible.  
 348 Frequencies between these bounds contain a mixture of flow noise and ambient noise. This explains why  
 349 the coherence critical frequencies are noticeably higher than those of the spectral method. The application  
 350 of spectral and coherence critical frequencies provides insight on the relative extent of both ambient noise  
 351 and flow noise within a signal.

### 352 C. Beamforming

353 The linear array can be effectively treated as one sensor or hydrophone using broadside beamforming.  
 354 This method generates signals that represent the coherent output of the entire array. These signals can  
 355 be compared to a single fixed hydrophone using spectral analysis, as shown in Fig. 7. The results of  
 356 this analysis reveal relatively lower spectral critical frequencies for the array, suggesting that the coherent  
 357 output from the array is less affected by flow noise and contains a greater extent of ambient noise.

358 This interpretation is supported by a visual comparison of signals from the coherent array, a fixed single  
 359 hydrophone, and the GuardBuoy (Fig. 8). The beamformed array contains lower levels at low frequencies

360 and a lower spectral critical frequency than the fixed single hydrophone. The difference in signal levels  
361 between the coherent array and the fixed single hydrophone implies moderate flow noise suppression.  
362 Furthermore, the slight improvement in spectral critical frequency indicates that coherent averaging has  
363 enhanced the measurement of ambient noise.

364 It is important to note that the improvements in signal level and spectral critical frequency illustrated  
365 in Fig. 7 and Fig. 8 are limited in magnitude. Further research would help determine the effectiveness  
366 of the coherent array as a method of flow noise suppression. This includes longer deployment periods,  
367 testing in different flow conditions, and experimentation in different bathymetric settings. Elimination of  
368 the mechanical noise floor would strengthen the present research. It would also be helpful to conduct tests  
369 with arrays of different length and a varied number of elements.

370

## VI. CONCLUSION

371 Flow noise appears as:  $f^{-5/3}$  noise when wavelength  $\gg$  sensor size, and  $f^{-m}$  noise, where the  
372 sensor's finite dimension reduces the flow noise. The steepened slope,  $f^{-m}$ , is related to the flow speed  
373 over the array. The spectral critical frequency is used to identify where ambient noise is negligible and  
374 the coherence critical frequency is used to identify where flow noise is negligible.

375 Coherent processing (beamforming) yields lower levels at low frequencies and a lower spectral critical  
376 frequency relative to a fixed single hydrophone. These improvements suggest that coherent processing  
377 could become an effective method of flow noise suppression. Experimentation in different flow settings  
378 and testing different array configurations would help determine the effectiveness of this approach.

379

## REFERENCES

- [1] R. Karsten, A. Swan, and J. Culina, "Assessment of arrays of in-stream tidal turbines in the Bay of Fundy," *Phil. Trans. R. Soc. A*, vol. 371, no. 1985, p. 20120189, 2013.
- [2] Z. Yang and A. Copping, *Marine Renewable Energy: Resource Characterization and Physical Effects*. Springer, 2017.
- [3] R. Inger, M. J. Attrill, S. Bearhop, A. C. Broderick, W. James Grecian, D. J. Hodgson, C. Mills, E. Sheehan, S. C. Votier, M. J. Witt *et al.*, "Marine renewable energy: potential benefits to biodiversity? An urgent call for research," *Journal of Applied Ecology*, vol. 46, no. 6, pp. 1145–1153, 2009.
- [4] B. Polagye, B. Van Cleve, A. Copping, and K. Kirkendall, "Environmental effects of tidal energy development: Proceedings of a scientific workshop," US National Oceanographic and Atmospheric Administration, Tech. Rep., 2011.
- [5] M. J. Dadswell, "Occurrence and migration of fishes in Minas Passage and their potential for tidal turbine interaction," 2010.
- [6] A. Redden and M. Stokesbury, "Acoustic tracking of fish movements in the Minas Passage and FORCE demonstration area: Pre-turbine baseline studies (2011-2013)."
- [7] A. Copping, N. Sather, L. Hanna, J. Whiting, G. Zydlewski, G. Staines, A. Gill, I. Hutchison, A. OHagan, T. Simas *et al.*, "Annex IV 2016 state of the science report: Environmental effects of marine renewable energy development around the world," *Ocean Energy Systems*, 2016.
- [8] G. D. Hastie, D. J. Russell, P. Lepper, J. Elliott, B. Wilson, S. Benjamins, and D. Thompson, "Harbour seals avoid tidal turbine noise: implications for collision risk," *Journal of Applied Ecology*, 2017.
- [9] D. Wang, M. Atlar, and R. Sampson, "An experimental investigation on cavitation, noise, and slipstream characteristics of ocean stream turbines," *Proceedings of the Institution of Mechanical Engineers, Part A: Journal of Power and Energy*, vol. 221, no. 2, pp. 219–231, 2007.
- [10] A. Lombardi, "Soundscape characterization in Grand Passage, Nova Scotia, a planned in-stream tidal energy site," 2016.
- [11] M. Lighthill, "The Bakerian lecture, 1961. Sound generated aerodynamically," in *Proceedings of the Royal Society of London A: Mathematical, Physical and Engineering Sciences*, vol. 267, no. 1329. The Royal Society, 1962, pp. 147–182.
- [12] M. Strasberg, "Nonacoustic noise interference in measurements of infrasonic ambient noise," *The Journal of the Acoustical Society of America*, vol. 66, no. 5, pp. 1487–1493, 1979.
- [13] V. O. Knudsen, R. Alford, and J. Emling, "Underwater ambient noise," *J. Mar. Res.*, vol. 7, pp. 410–429, 1948.
- [14] C. Bassett, J. Thomson, P. H. Dahl, and B. Polagye, "Flow-noise and turbulence in two tidal channels," *The Journal of the Acoustical Society of America*, vol. 135, no. 4, pp. 1764–1774, 2014.
- [15] D. R. Barclay and M. J. Buckingham, "Depth dependence of wind-driven, broadband ambient noise in the Philippine Sea," *The Journal of the Acoustical Society of America*, vol. 133, no. 1, pp. 62–71, 2013.
- [16] J. Chung, "Rejection of flow noise using a coherence function method," *The Journal of the Acoustical Society of America*, vol. 62, no. 2, pp. 388–395, 1977.
- [17] B. M. Buck and C. R. Greene, "A two-hydrophone method of eliminating the effects of nonacoustic noise interference in measurements of infrasonic ambient noise levels," *The Journal of the Acoustical Society of America*, vol. 68, no. 5, pp. 1306–1308, 1980.
- [18] F. Dupont, C. G. Hannah, and D. Greenberg, "Modelling the sea level of the upper Bay of Fundy," *Atmosphere-Ocean*, vol. 43, no. 1, pp. 33–47, 2005.
- [19] B. Wilson, R. S. Batty, and L. M. Dill, "Pacific and atlantic herring produce burst pulse sounds," *Proceedings of the Royal Society of London B: Biological Sciences*, vol. 271, no. Suppl 3, pp. S95–S97, 2004.

- 417 [20] J. A. Hildebrand, "Anthropogenic and natural sources of ambient noise in the ocean," *Marine Ecology Progress Series*, vol. 395, pp.  
418 5–20, 2009.
- 419 [21] N. D. Merchant, T. R. Barton, P. M. Thompson, E. Pirotta, D. T. Dakin, and J. Dorocicz, "Spectral probability density as a tool for  
420 ambient noise analysis," *The Journal of the Acoustical Society of America*, vol. 133, no. 4, pp. EL262–EL267, 2013.
- 421 [22] M. J. Buckingham, "On the two-point cross-correlation function of anisotropic, spatially homogeneous ambient noise in the ocean and  
422 its relationship to the Green's function," *The Journal of the Acoustical Society of America*, vol. 129, no. 6, pp. 3562–3576, 2011.
- 423 [23] B. F. Cron and C. H. Sherman, "Spatial-correlation functions for various noise models," *The Journal of the Acoustical Society of  
424 America*, vol. 34, no. 11, pp. 1732–1736, 1962.
- 425 [24] G. B. Deane, M. J. Buckingham, and C. T. Tindle, "Vertical coherence of ambient noise in shallow water overlying a fluid seabed,"  
426 *The Journal of the Acoustical Society of America*, vol. 102, no. 6, pp. 3413–3424, 1997.
- 427 [25] H. Cox, "Line array performance when the signal coherence is spatially dependent," *The Journal of the Acoustical Society of America*,  
428 vol. 54, no. 6, pp. 1743–1746, 1973.

429 **Matthew Auvinen** Biography text here.

PLACE  
PHOTO  
HERE

430

431 **David Barclay** Biography text here.

PLACE  
PHOTO  
HERE

432